Finite element simulation of an injection moulding process

D. Ding, P. Townsend and M.F. Webster
University of Wales Institute of non-Newtonian Fluid Mechanics, Department of Computer Science, University of Wales Swansea, UK

Received June 1996
Revised November 1996

Introduction

This study reports our experiences in simulating an injection moulding process, and in particular the filling of a thin-walled cup-shaped mould with a polystyrene material. The process is highly thermally convective, with the hot injected polymer being cooled by the mould walls as the filling proceeds. Characterization of the material has been undertaken at the Technology University of Eindhoven, forming part of a project in which technology has been developed combining an experimental-simulation study. This is directed towards multi-layer injection moulding, where multiple materials may be simultaneously or sequentially injected into a mould.

A finite element simulation code is employed which has the facility to track fluid particles, moving fronts and deformation patterns throughout the filling process. This is a dynamic operation, that involves a continually expanding wetted domain and demands the use of a transient algorithm. A Taylor-Galerkin/pressure-correction time-stepping scheme is invoked for this purpose. A full generalized Newtonian treatment is taken, capable of extension into three dimensions, involving an energy equation for the transport of temperature as discussed in[1-3]. A shear-thinning model is adopted and viscous dissipation is taken into account.

In the literature, a Hele-Shaw approximation[4] has been used widely to simulate the injection moulding process, and was originally developed for slow flows under isothermal conditions. The key assumption of this approach is that a constant pressure applies in the gapwise direction (z), between two parallel planes (x-y) with vanishing velocity normal to the principal flow direction. Hence, the pressure field can be resolved in two dimensions, i.e. across the mid-plane between the parallel planes, and the velocity field may be integrated analytically across the gap between the planes. Richardson[5] first described this approach as a lubrication approximation, in a cavity mould filling operation. Williams and Lord[6] and Lord and Williams[7] employed a finite difference method to predict the non-isothermal temperature distribution in the

Financial support from the Commission of the European Communities is gratefully acknowledged (Contract BREU-495-BRITE/EURAM, Project BE-4076).

International Journal for Numerical Methods for Heat & Fluid Flow
Vol. 7 No. 7, 1997, pp. 751–766.

gapwise direction for filling cavity-shaped moulds, including a sprue, runner and gate system. Their simulation was restricted to flow in a straight channel. Hieber and Shen[8] introduced a finite element/finite difference formulation for the filling of thin-walled shaped moulds, in which the mid-plane (x-y) is discretized by finite elements, with the gapwise and time derivatives discretized by finite differences. This approach is inappropriate for thick-walled moulds, where the flow front does not maintain a flat shape. Vos *et al.*[9] proposed a multilayer injection moulding technique, again with recourse to a Hele-Shaw approximation. The flow front consequently flattens, so that fountain flow cannot be predicted in the z-direction across the gap of the mould. To capture the important heat advection effects in the gapwise direction, Crochet *et al.*[10] studied filling problems for arbitrary shaped-cavities with a Hele-Shaw approach. Although the pressure and temperature fields are solved following Hieber and Shen[8], special consideration is given to the thermal conditions at the flow front to address the onset of fountain flow. That is the temperature distribution at the flow front is consistent with the streamlines. This is a major improvement, but again it is not applicable for thick-walled moulds because the flow front is restricted to a flat surface in the z-direction. Mavridis *et al.*[11] developed a transient free-surface scheme to model the motion of the front and simulate fountain flow. In their work, a moving contact line is introduced where the free surface intersects a stationary boundary. The location of this intersection influences the extent of application for the no-slip boundary condition up to the contact line, where a stress singularity results. A three-dimensional boundary element approximation was recently reported by Khayat *et al.*[12] for gas-assisted injection moulding. The drawback to this method is that the boundary integral technique is limited and not easily extended to non-linear systems. A so-call fringe element generation method was proposed by Sato and Richardson[13] for viscoelastic materials in a moulding process under isothermal condition. This method is a localized mesh regeneration technique, that effects adjustments only in the neighbourhood of the front, as opposed to a complete domain remesh. It is similar to a source propagation method in tracing an advancing flow front, cited by Sitters[14] and employed in the present work. On the experimental side, Schmidt[15] used colour tracers to visualize the fluid deformation patterns and fountain flow. Similar results have been reported also by Coyle *et al.*[16] and Chu *et al.*[17].

Of critical importance is the tracking of the moving front as the polymer melt fills the mould (the orientation and shape it adopts), and the location of particle bands behind the front. The deformation patterns of the polymeric bands that are traced out during the filling and cooling process may ultimately be used in an inverse operation, to dictate when and where to inject bands of material, so as to realize a layered configuration. In a complex shaped mould, this process is non-trivial, due to the rheological complexity and processing conditions involved. Yet often a single injection step is necessary in order to achieve this multi-layered form. The present analysis goes some way to establishing this technology by considering truly thin-walled moulds, studying the motion of

individual injected material bands, the tracking of melt fronts and the changes in material and flow properties whilst processing. A thin-walled cup shaped mould is considered, which is illustrated schematically in Figure 1. The flow domain comprises three parts:

(1) an entry tube with radius of 1.5mm at the inlet and 3mm at the first re-entrant corner and length of 15mm;

(2) a disc-shaped region of 30mm radius and 3mm thickness; and

(3) an annular region of 34mm outer radius at the edge of the cup, 42mm beyond the disk and 3mm thickness.

The operating conditions are an entry melt temperature T_0 = 503 °K, a mould wall temperature T_{wall} = 330 °K and a flowrate Q = 0.034cm^3/sec.

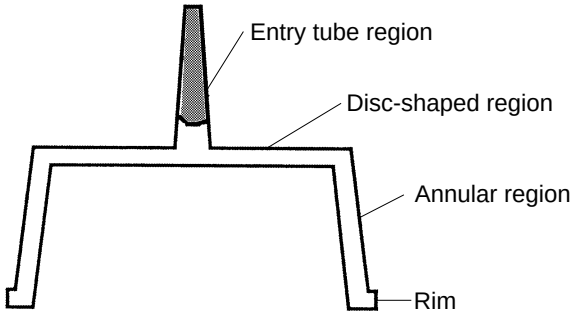

Figure 1.
Schematic diagram for filling thin-walled cup

Governing equations

The relevant equations governing such flows are the generalized momentum and energy equations for inelastic fluids under incompressible and non-isothermal conditions, but in the absence of forcing functions. These equations may be expressed as

$$\rho \mathbf{u}_t = \nabla.(\mu \nabla \mathbf{u}) - \rho \mathbf{u}.\nabla \mathbf{u} - \nabla p \tag{1}$$

$$\nabla.\mathbf{u} = 0 \tag{2}$$

$$\rho c_p T_t = \nabla.(\kappa \nabla T) - \rho c_p \mathbf{u}.\nabla T - \mu \Phi \tag{3}$$

where u = u($\mathbf{x}$, t), p = p($\mathbf{x}$, t) and T = T($\mathbf{x}$, t) are velocity, pressure and temperature with dependence on space $\mathbf{x}$ and time t, subscript t denotes $\frac{\partial}{\partial t}$, ρ is the density taken as 1000kg/m^3, μ is the shear viscosity, c_p is the heat capacity at constant pressure taken as 1800 J/°K/kg, κ is the thermal conductivity taken as 0.16 W/m/°K, and Φ is the viscous dissipation, a function of the second invariant of the rate-of-strain tensor I_2. In particular, $\Phi = \frac{1}{2} I_2$. A Carreau-Yasuda model, represents the viscosity behaviour as

$$\mu = K_1[1 + (K_2\gamma)^2]^{\frac{m-1}{2}} \tag{4}$$

with

$$K_1 = B_1 e^{\frac{A_1}{T}}, \tag{5}$$

$$K_2 = B_2 e^{\frac{A_2}{T}}, \tag{6}$$

where γ is the shear rate, m is the power-law index taken as 0.48; A_1, A_2, B_1, B_2 are material constants taken as $A_1 = 11130$ °K, $A_2 = 11390$ °K , $B_1 = 9.23 \times 10^{-7}$ Pa.sec , and $B_2 = 6.69 \times 10^{-11}$ sec. A glass transition temperature $T_g = 370$ °K is adopted in the near wall vicinity, at which a Newtonian viscosity plateau is imposed to model the localized highly viscous attenuation.

A schematic representation for a pipe-shaped mould in Figure 2 illustrates a typical flow domain portion, to which the following boundary conditions are applied,

inlet (Γ_1): $\mathbf{u} = (v_r, v_z)$ and T prescribed as $v_r = 0$, $v_z = v_z(r)$ and $T = T_{melt}$,

walls (Γ_2): no-slip, $v_r = v_z = 0$ and $T = T_{wall}$,

symmetry (Γ_4): $v_r = 0$, $\tau_{rz} = 0$ and $\frac{\partial T}{\partial s} = 0$,

front (Γ_3): $(\tau - \delta p).s = 0$ and $\frac{\partial T}{\partial s} = 0$,

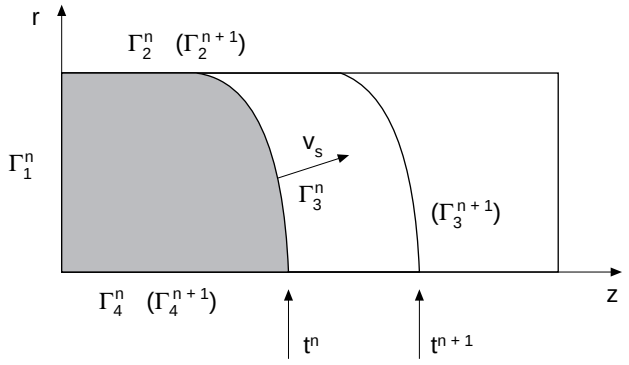

Figure 2.
Flow domain and moving boundaries

where a boundary Γ_i has a time level superscript of either n or n + 1. v_r and v_z are the radial and axial velocity components respectively, τ is a stress tensor, δ is a unit tensor, T_{melt} and T_{wall} are the melt and wall temperature respectively, and s is an outward pointing normal to the boundaries Γ_3 or Γ_4.

The flow problem is categorized through dimensionless groups of Reynolds number, Re, thermal Peclet number, Pe, and Griffith number, Gf, defined as

$$Re = \frac{\rho LV}{\mu_o}, \tag{7}$$

$$Pe = \frac{\rho c_p LV}{\kappa}, \tag{8}$$

$$Gf = \frac{\mu_o V^2}{\kappa A_1}, \tag{9}$$

where L is a characteristic length scale, taken as the radius of the mould at the injecting point, V is a characteristic velocity, taken as a mean velocity at the injecting point, and μ_o is a reference viscosity associated with a zero shear rate and a reference temperature of the inlet melt flow. A characteristic time scale is then $\frac{L}{V}$. Here the magnitude of Re relates to the inertia in the flow, while that of Pe shows the importance of thermal convection to conduction, and Gf describes the temperature increase due to viscous heating. Taking viscosity scaled with respect to μ_o, equations (1-3) may be interpreted non-dimensionally in the form:

$$Re\,\mathbf{u}_t = \nabla.(\mu\nabla\mathbf{u}) - Re\,\mathbf{u}.\nabla\mathbf{u} - \nabla p \tag{10}$$

$$\nabla.\mathbf{u} = 0 \tag{11}$$

$$T_t = \frac{1}{Pe}\nabla^2 T - \mathbf{u}.\nabla T - \frac{Gf}{Pe}\mu\Phi \tag{12}$$

The magnitude of those dimensionless groups are Reynolds number Re = 3.84×10^{-6}, thermal Peclet number Pe = 162, Griffith number Gf = 4.31×10^{-3} and $\frac{Gf}{Pe} = 2.66 \times 10^{-5}$. These are model representations of typical physical processing conditions, where Pe may range from $O(10^3)$ to $O(10^5)$.

Numerical scheme

Based on a semi-implicit Taylor-Galerkin finite element method discussed in Hawken *et al.*[18], and extended to a thermal context by Ding *et al.*[1], equations (10)-(12) are discretized first in time according to a Taylor series prior to a Galerkin spatial discretization. The pressure equation is decoupled from the momentum equation through a projection method. This leads to a Poisson equation to solve for the pressure, which in turn is used to correct the velocity solution. To aid stability, an implicit treatment for diffusion is adopted for both momentum and energy equations. Solutions are then obtained through fractional stages within each time step. The fully discretized forms for the semi-implicit Taylor-Galerkin/pressure correction scheme over a time step $\Delta t = t^{n+1} - t^n$ may be expressed as:

Stage 1a:

$$[\frac{2\,Re}{\Delta t}M + \frac{1}{2}S_u](U^{n+\frac{1}{2}} - U^n) = \{-[S_u U + Re\,N(U)U] + L^T P\}^n \tag{13}$$

$$[\frac{2}{\Delta t}M + \frac{1}{2Pe}S_T](T^{n+\frac{1}{2}} - T^n) = \{-[\frac{1}{Pe}S_T T + N(U)T] + \frac{Gf}{Pe}\mu\Phi(U)\}^n, \quad (14)$$

Stage 1b:

$$[\frac{Re}{\Delta t}M + \frac{1}{2}S_u](U^* - U^n) = [-S_u U + L^T P]^n - Re[N(U)U]^{n+\frac{1}{2}}, \quad (15)$$

$$[\frac{1}{\Delta t}M + \frac{1}{2Pe}S_T](T^{n+1} - T^n) = -\frac{1}{Pe}S_T T^n + [-N(U)T + \frac{Gf}{Pe}\mu\Phi(U)]^{n+\frac{1}{2}}, \quad (16)$$

Stage 2:

$$K(P^{n+1} - P^n) = -\frac{2}{\Delta t}LU^*, \quad (17)$$

Stage 3:

$$\frac{Re}{\Delta t}M(U^{n+1} - U^*) = \frac{1}{2}L^T(P^{n+1} - P^n), \quad (18)$$

where $\mathbf{U}^n$, $\mathbf{P}^n$ and $\mathbf{T}^n$ are nodal vectors at time t^n for velocity, pressure and temperature respectively; $\mathbf{U}^*$ is an intermediate non-solenoidal nodal velocity vector introduced in step 1a; M, S_U, S_T, N(U), K and L are mass matrix, momentum diffusion matrix, thermal diffusion matrix, convection matrix, pressure stiffness matrix and divergence/pressure gradient matrix respectively; Φ is the nodal dissipation vector. The above notation may be interpreted at the component level, through quadratic functions ϕ_k and linear functions ψ_k defined continuously on a triangular tessellation of the domain, as

$$M(i,j) = \int_\Omega r\phi_i\phi_j d\Omega, \quad (19)$$

$$N(i,j) = \int_\Omega r\phi_i(U_k^l\phi_l\frac{\partial\phi_j}{\partial x_k})d\Omega, \quad (20)$$

$$K(i,j) = \int_\Omega r(\nabla\psi_i \cdot \nabla\psi_j)d\Omega, \quad (21)$$

$$L_k(i,j) = \int_\Omega r\phi_i\nabla_k(\phi_j)d\Omega, \quad (22)$$

$$S_u(i,j) = (S_{lm})_{ij}, \qquad l, m = 1, 2, \quad (23)$$

$$S_{11}(i,j) = \int_\Omega r\mu(2\frac{\partial\phi_i}{\partial r}r + \frac{\partial\phi_i}{\partial z}\frac{\partial\phi_j}{\partial z} + 2\frac{\phi_i\phi_j}{r^2})d\Omega, \quad (24)$$

$$S_{12}(i,j) = \int_{\Omega} r\mu\left(\frac{\partial \phi_i}{\partial z}\frac{\partial \phi_j}{\partial r}\right)d\Omega\,, \tag{25}$$

$$S_{21}(i,j) = S_{12}(i,j) \tag{26}$$

$$S_{22}(i,j) = \int_{\Omega} r\mu\left(\frac{\partial \phi_i}{\partial r}\frac{\partial \phi_j}{\partial r} + 2\frac{\partial \phi_i}{\partial z}\frac{\partial \phi_j}{\partial z}\right)d\Omega \tag{27}$$

$$S_T(i,j) = \kappa\int_{\Omega} r\left(\nabla\phi_i \cdot \nabla\phi_j + \frac{\phi_i}{r}\frac{\partial \phi_j}{\partial r}\right)d\Omega \tag{28}$$

$$\Phi(i) = \frac{1}{2}\int_{\Omega} r\mu\phi_i\left[\left(\frac{\partial \phi_m}{\partial x_k}U_l^m + \frac{\partial \phi_m}{\partial x l}U_k^m\right)^2 + 2\left(\frac{\phi_m}{r}U_r^m\right)^2\right]d\Omega\,,\ k,\ l = 1,\ 2. \tag{29}$$

A Crank-Nicolson splitting of pressure terms over time is used giving the above pressure-correction representation. The algebraic systems that emerge are solved using both direct and iterative techniques. All mass-matrix based equations are solved with an element-wise Jacobi iteration, using mass-lumping to enhance stability[19]. The pressure equation is solved through a Choleski method using a bandwidth reduction strategy.

Front tracking

In the literature, a free surface technique was developed by Mavridis *et al.*[11] to trace the transient advancement of the flow front during the injection moulding process. From the point of view of mass conservation, a free surface is a material surface across which fluid does not pass. To maintain the motion of the free surface, a contact line theory was employed, where the free surface intersects a solid wall. The contact line appears to move as new material reaches the wall from the free surface, leading to a stress singularity when a no-slip condition is applied at the wall. This issue is avoided in our approach as the wall contact point is taken as fixed, only to be relocated at discrete moments in time when the front proximity to the wall is sufficiently close.

A so-called source propagation scheme is employed in this paper for front tracking. The scheme is based on Huygens' principle from the theory of light propagation, that is, a point source can fill an area with a radius proportional to its strength. Following this principle, a source propagation technique was employed by Sitters[14] to model the movement of the flow front during a filling operation. Here, this scheme has been updated for triangular finite element meshes shown schematically in Figure 3. The shaded domain indicates a filled wet zone and the unshaded region indicates a dry region, yet to be filled. Solid lines constitute a fixed background mesh over the domain, and dashed lines indicate where local remeshing is to be performed.

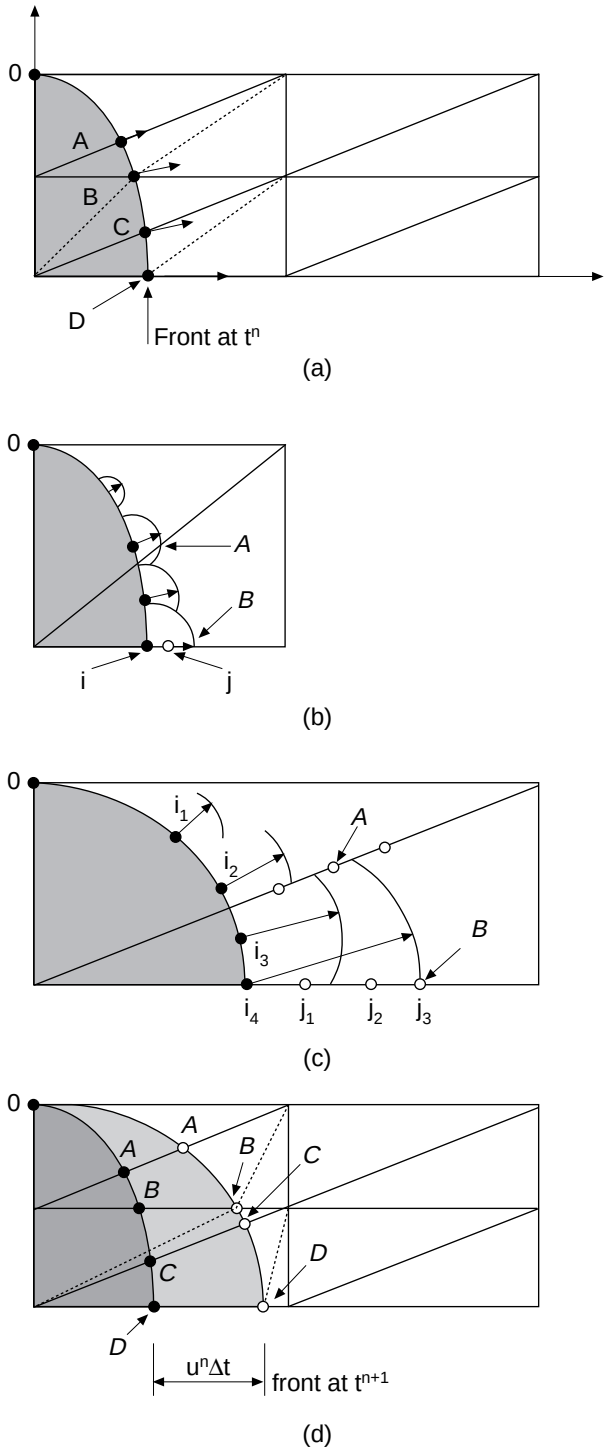

Figure 3.
Illustration of source propagation scheme

A source point has dual attributes of mass and velocity, with the latter relating to how far the front will swell in a fixed time. Candidate source point velocities are sampled on the current front and their projected swelling distances are calculated, with respect to intersection on the background mesh local to the front. A flow front is therefore considered as a series of point sources, that are indicated as arcs of circles in Figure 2. The strength of these point sources is proportional to their normal velocity $|\mathbf{u}|$, as shown by arrow in Figure 3a. On an element of the background mesh, the dry part of an element edge that intersects with the front is delineated by a series of edge points. This is for the purpose of recording the limits of filling over the edge for the time step. Then, an edge point j (indicated by o) can be filled by a point source i (e.g. A, B, C, D shown as •), located in the same element, if $(|\mathbf{u}_i|\Delta t - d_{ij}) > 0$. Here d_{ij} is the distance between points i and j as shown in Figure 3b. The filled edge point j then becomes a new point source and its strength is given by $\max[(|\mathbf{u}_i|\Delta t - d_{ij})/\Delta t]$ for all point sources i. The strongest source point will wet the furthest edge points along any particular edge, as in Figure 3c. This then delimits the perimeter of the wet mesh to be adopted at the end of the filling time step. The procedure is repeated for all background elements containing flow front segments providing an updated front position OAB as shown in Figure 3b and 3c, where A and B indicate new front intersections with the background mesh.

Local remeshing, performed around the flow front based on the background mesh, generates a new wet mesh, as shown in Figure 3d with updated front location ABCD denoted by o. This scheme has the advantage that it accommodates for flow around sharp corners. It is less appropriate for convection dominated problems, since the filling process centred at each candidate filling point is assumed to be uniform in all directions. An aside is that source propogation is complicated to implement, owing to the intricacies involved in local remeshing, and projection onto the background mesh each occasion a new front position is located.

With an updated wet mesh, the Taylor-Galerkin algorithm is invoked to evaluate the temporal increment over $[t^n, t^{n+1}]$ of the solution on the field. This step enforces mass conservation on the updated mesh up to the later time t^{n+1}. As the flow front progresses from one position at tn, to a second at t^{n+1}, the imposed boundary conditions on the field equations are adjusted. The momentum traction boundary conditions are homogeneous and arise naturally in the problem formulation for both wet and dry front positions. The imposed homogeneous Neumann boundary conditions on the Poisson pressure difference equation still remain, as we can take $\mathbf{u}^*$ to equal $\mathbf{u}^{n+1}$ on the larger domain boundary at t^{n+1}. This implies therefore that the boundary condition term for this equation in weak form is:

$$R = \oint_{\Gamma^{n+1}} \psi_i \nabla(p^{n+1} - p^n).\mathbf{s}\,d\Gamma$$

taking the extended definition of ∇p^n over the wider domain with the boundary

specified by Γ^{n+1} at t^{n+1}. This is true, as the pressure gradient term ∇p^n must vanish on the dry part of the mesh, that is subsequently filled over the interval $[t^n, t^{n+1}]$. To further enhance temporal accuracy we have also adopted a sub-time stepping technique, an iterative correction scheme, to solve the field equations for each estimated new front position. Based on an initial empirical estimation we have formed a fixed number of sub-time steps of say ten to 15. This approach corrects for inaccuracies that can arise in a crude estimation of front position and solution of the dynamic flow equations.

For problems with a complicated geometry, for example involving a corner in the domain, the following criteria prove of assistance as shown in Figure 4. If a flow front OABCD at time t^{n+1} crosses a fixed re-entrant corner P, take OAPBCD instead of OABCD as shown in Figure 4a. This gives rise to two segments of the current front OAP prior to corner P, and PBCD beyond P, each to be dealt with independently. For a front segment PBC that has advanced some way beyond the corner P, there are some additional heuristics to consider. For precision in front location, there is now not only the proximity of particle B to the wall to adjust for, but also we must limit the extension of the front portion PB. As shown in Figure 4b, if the distance between particle B at the front PBC and the wall satisfies $\delta_z < \delta_{min}$, or the extension of PB exceeds a predefined limit as governed through $\delta_r > \delta_{max}$, then adopt ABC in place of PBC for the current front location by extrapolation to the wall.

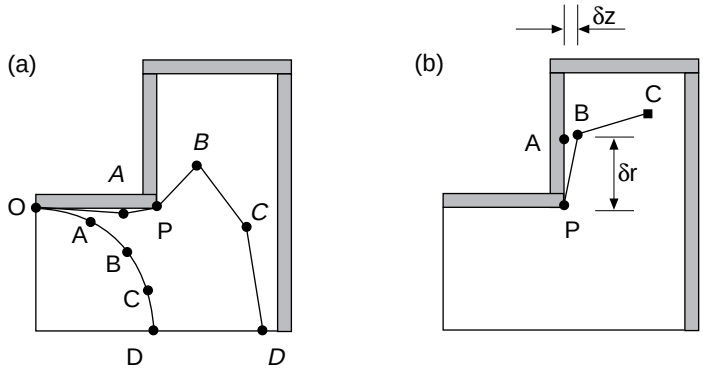

Figure 4.
Front adjustment of flow around a corner

Particle tracking

As it is important to track material deformation (through movement of bands) and particle histories behind the flow front during the filling process, it is necessary to incorporate a particle tracking technique. A well established Runge-Kutta scheme is adopted, which can be written as an explicit Euler step:

$$^{p}\mathbf{x}_i^{n+1} = \mathbf{x}_i^n + \Delta t \mathbf{u}(\mathbf{x}_i, t^n) \tag{30}$$

and an averaged correction step:

$$^{c}\mathbf{x}_i^{n+1} = \mathbf{x}_i^n + \frac{1}{2}\Delta t[\mathbf{u}(\mathbf{x}_i, t^n) + (^{p}\mathbf{x}_i, t^{n+1})] \tag{31}$$

where, for a particle denoted by i, $\mathbf{x}_i^n$ is its location at time t^n, ${}^p\mathbf{x}_i^{n+1}$ is a predicted particle position at time t^{n+1}, ${}^c\mathbf{x}_i^{n+1}$ is a corrected position at time t^{n+1}, $\mathbf{u}(\mathbf{x}_i, t^n)$ is the particle velocity at time t^n, $\mathbf{u}({}^p\mathbf{x}_i, t^{n+1})$ is the particle velocity at a predicted position ${}^p\mathbf{x}_i^{n+1}$ at time t^{n+1}. This scheme is performed after stage 3 of each time step of the Taylor-Galerkin algorithm, as described in section 2.

Figure 5 shows this tracking procedure schematically. For practical convenience, a small gap is introduced between the first particle and the wall of the mould to avoid the difficulty of dealing with stationary particles. To maintain a uniform particle distribution along the band, it is appropriate to update the position of neighbouring particles according to the average distance between any two particles. The position of particles along the band may be relocated if their neighbouring separation distances (δ) exceed limiting criteria, such as $\delta > \delta_{max}$ or $\delta < \delta_{min}$ where $\delta_{max} = 1.5\ \delta_{average}$ and $\delta_{min} = 0.5\ \delta_{average}$. This naturally invokes a dynamic readjustment of the particle positions. These strategies may be modified to best suit the particular problem in hand.

Numerical results

The simulation is based on a finite element mesh as shown in Figure 6, which involves 944 triangular elements, 2,133 velocity/temperature nodes and 595 pressure nodes, giving 6,994 degrees of freedom in total. The boundary

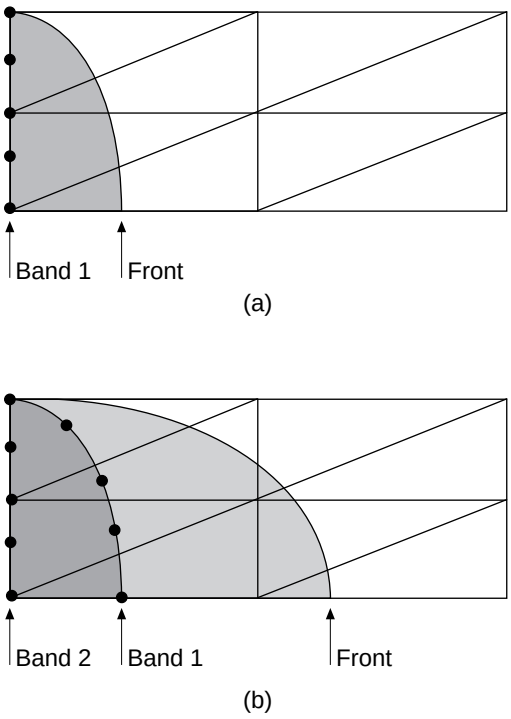

Figure 5.
Particle tracking for material bands at times (a) t^1, (b) t^2

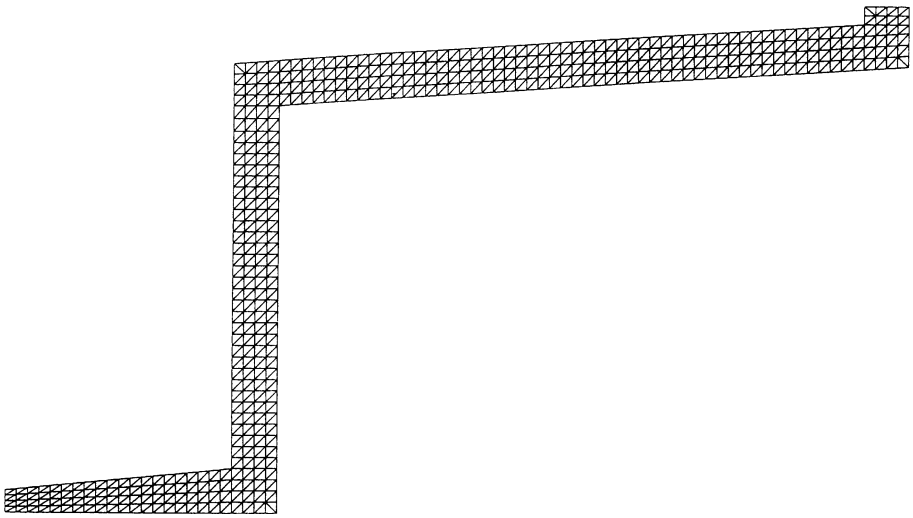

Figure 6.
A finite element mesh for a thin-walled cup

conditions of the flow domain are defined in section 2, where the melt temperature at the injection point, i.e. the inlet of the flow domain, is taken as T_o = 503 °K, the wall temperature of the mould is fixed as T_{wall} = 330 °K and an adiabatic condition is applied to the flow front throughout the whole process. In order to trace the material deformation pattern accurately, 2,000 particles are employed for each band.

As described above, the thermal Peclet number employed is about $Pe = 10^2$. In practice $Pe = 10^5$ is not uncommon, and this study is intended to provide insight and guidance for these more realistic conditions. Figure 7 shows the movement of the flow front and the deformation patterns of the material bands during the filling process at dimensionless times $t_1 = 1$, $t_2 = 16$, $t_3 = 32$, $t_4 = 43$, $t_5 = 70$ and $t_6 = 105$. The flow front smoothly negotiates the entry tube region into the disc-shaped region and the re-entrant corner into the annular region, before finally reaching the rim region. Compared with the results for a thick-walled cup[20], as shown in Figure 8 at times $t_1 = 5$ through $t_8 = 55$, a fountain flow pattern is barely discernible, owing to the relatively thin-walled dimensions of the cup. The pressure gradient in the cross flow direction is almost constant as the filling progresses, so that fountain flow is suppressed. Alternatively, we have observed a fountain flow in the filling of a thick-walled cup as shown in Figure 8, where the pressure gradient is significant in the gapwise (thickness) direction. These results are physically reasonable and consistent in deformation patterns with examples cited in the literature, covering similar flow configurations with fountain flow and filling[14-16,21,22].

Figure 9 shows the temperature contour plot during the filling process, where lighter shades of grey imply hotter material. The plot indicates that heat is strongly convected into the mould, as the melt is injected. This is due to the relatively large value of thermal Peclet number and the effect of cooling (the hot

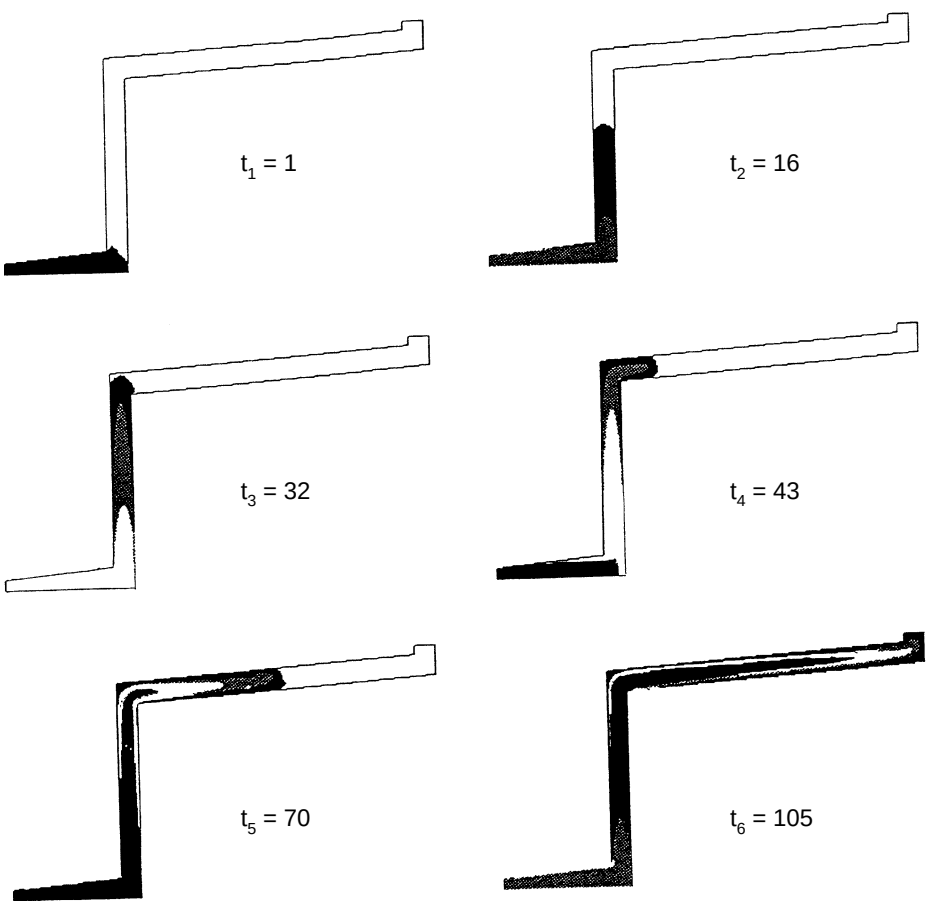

Figure 7.
Deformation patterns for filling of a thin-walled cup

melt at the injection point and cold mould wall). Heat convection continues, but weakens as the melt progresses along the disc-shaped region, and finally disappears after the melt has passed beyond the second re-entrant corner and entered the annular region. This may be explained by a significant reduction in local filling speed, as the melt fills the disc-shaped zone and the radius of the wet domain increases. At the same time the flowrate at the injection point remains constant.

Concluding remarks

Here, we have successfully demonstrated the use of a numerical inelastic flow solver as a prediction tool for the filling phase of an injection moulding process. We have been able to accommodate thin-walled moulds and provide physically realistic simulations for this complex cooling process using inelastic fluid models. An accurate localized remeshing and front tracking technique has been implemented effectively and material deformation patterns have been presented.

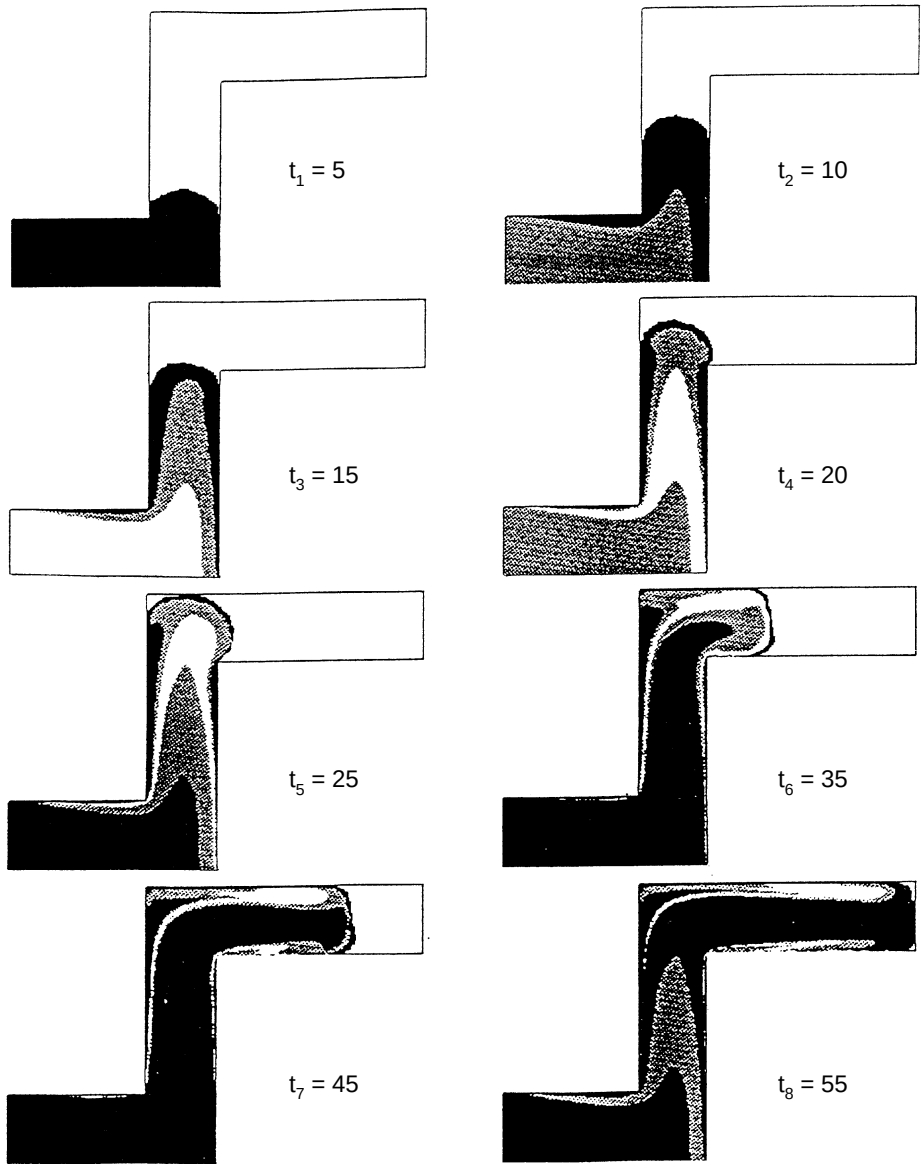

Figure 8.
Deformation patterns for filling of a thick-walled cup

As the thermal Peclet number grows to $O(10^5)$, with shorter injection times and larger velocities, the problem becomes significantly more thermally convective. This will have a marked effect within the thermal boundary layers on the mould walls, reducing their width. Owing to the thin-walled nature of the mould here, such sharp solution gradients present a formidable challenge to any numerical scheme to capture accurately. The convection-diffusion problem itself introduces non-trivial numerical challenges, as the convection increasingly

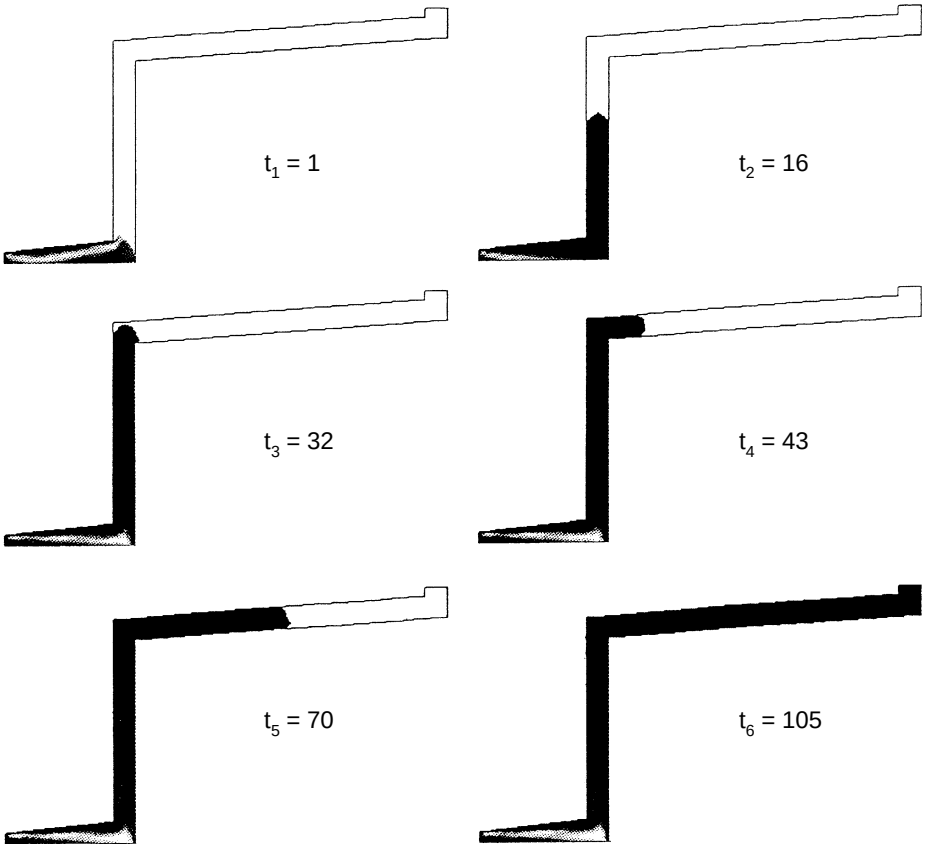

Figure 9.
Temperature contour plots for filling of a thin-walled cup

dominates. This will require sophisticated additional numerical strategies to resolve successfully these extended ranges of working conditions. It is intended to implement streamline upwind weighting to attack such severe demands with careful attention to mesh resolution in cross-stream directions to capture the thermal boundary layers.

Promising future directions of research on this topic are as follows. Three-dimensional calculations are a necessity for small-scale or complex shaped products. The implication are large-scale computations, that dictate the need for efficient robust solvers. Viscoelastic thermal rheological modelling is desirable for filling flows around complex geometrical mould shapes. Once multiple layered problems are resolved, experimentation with different injection sequences will be possible. The inverse problem of dictating the appropriate initial configuration of pre-injected material layers may then be attempted effectively.

References

1. Ding, D., Townsend, P. and Webster, M.F., "Computer modelling of transient thermal flows of non-Newtonian fluids", *J. Non-Newt. Fluid Mech.*, Vol. 47, 1993, pp. 239-65.

2. Ding, D., Townsend, P. and Webster, M.F., "The development of flow simulation software for polymer processing applications", *Revista Portuguesa De Hemorreologia*, Vol. 4, Suppl. 1/Pt A, 1990, pp. 31-38.
3. Ding, D., Townsend, P. and Webster, M.F., "On computation of two and three-dimensional unsteady thermal non-Newtonian flows", *Int. J. Num. Meth. Heat Fluid Flow*, Vol. 5 No. 6, 1995, pp. 495-510.
4. Schilighting, H., *Boundary-layer Theory*, McGraw-Hill, New York, NY, 1968.
5. Richardson, S., "Hele-Shaw flows with a free boundary produced by the injection of fluid into a narrow channel", *J. Fluid Mech.*, Vol. 56, 1972, pp. 609-18.
6. Williams, G. and Lord, H.A., "Mold-filling studies for the injection molding of thermoplastic materials. Part 1: The flow of plastic materials in hot- and cold-walled circular channels", *Polym. Eng. Sci.*, Vol. 15, 1975, p. 553.
7. Lord, H.A. and Williams, G., "Mold-filling studies for the injection molding of thermoplastic materials. Part 2: The transient flow of plastic materials in the cavities of injection-molding dies", *Polym. Eng. Sci.*, Vol. 15, 1975, p. 569.
8. Hieber, C.A. and Shen, S.F., "A finite-element/finite difference simulation of the injection molding filling process", *J. Non-Newt. Fluid Mech.*, Vol. 7, 1980, pp. 1-32.
9. Vos, E., Meijer, H.E.H. and Peters, G.W.M., "Multilayer injection moulding", *Int. Polym. Processing*, Vol. VI, 1991, pp. 42-50.
10. Crochet, M.J., Dupret, F. and Verleye, V., "Injection moulding", in Advani, S.G. (Ed.), *Flow and Rheology in Polymer Composites Manufacturing*, pp. 415-63, 1994.
11. Mavridis, H., Hrymak, A.N. and Vlachopoulos, J., "Transient free-surface flows in injection molding filling", *AIChE J.*, Vol. 34 No. 3, 1988, pp. 403-10.
12. Khayat, R.E., Derdouri, A. and Herbert, L.P., "A three dimensional boundary element approach for gas-assisted injection moulding", *J. Non-Newt. Fluid Mech.*, Vol. 57, 1995, pp. 253-70.
13. Sato, T. and Richardson, S.M., "Numerical simulation method for viscoelastic flows with free surfaces – fringe element generation method", *Int. J. Num. Meth. Fluids*, Vol. 19 No. 7, 1994, pp. 555-74.
14. Sitters, C.W.M., "Numerical simulation of injection moulding", PhD thesis, University of Technology, Eindhoven, 1988.
15. Schmidt, L.R., "A special mold and tracer technique for studying shear and extensional flows in a mold cavity during injection molding", *Polym. Eng. Sci.*, Vol. 14, 1974, pp. 797-800.
16. Coyle, D.J., Blake, J.W. and Macosko, C.W., "The kinematics of fountain flow in mold filling", *AICHE J.*, Vol. 33, 1987, pp. 1168-77.
17. Chu, E., Goyal, S.K. and Kamal, M.R., "Prediction of microstructure development during injection mold filling (The McKam-II model)", *SPE ANTEC Tec, Papers*, Vol. 45, 1987, p. 280.
18. Hawken, D.M., Tamaddon-Jahromi, H.R., Townsend, P. and Webster, M.F., "A Taylor-Galerkin based algorithm for viscous incompressible flow", *Int. J. Num. Meth. Fluids*, Vol. 10, 1989, pp. 327-51.
19. Ding, D., Townsend, P. and Webster, M.F., "The iterative solution of Taylor-Galerkin augmented mass matrix equations", *Int. J. Num. Meth. Eng.*, Vol. 35, 1992, pp. 241-53.
20. Ding, D., Townsend, P. and Webster, M.F., "Numerical simulation of filling problems related to injection moulding", in Dijksman, J.F. and Kuiken, G.D.C. (Eds), *IUTAM Symposium on Numerical Simulation of Non-isothermal Flow of Viscoelastic Liquids*, 1995, pp. 133-58.
21. Zoetelief, W., "Multi-component injection moulding", PhD thesis, University of Technology, Eindhoven, 1995.
22. Pearson, J.R.A., and Richardson, S.M., "Computational analysis of polymer processing", *Applied Science*, 1983.